A Thickness-Mode AlGaN/GaN Resonant Body High Electron Mobility Transistor

Azadeh Ansari, *Student Member, IEEE*, and Mina Rais-Zadeh, *Senior Member, IEEE*

***Abstract*— A multigigahertz AlGaN/GaN resonant body transistor (RBT) is reported, wherein the mechanical resonance and electrical signal modulation are achieved simultaneously. A 175-Å-thick AlGaN layer is used as the piezoelectric transduction layer, and the 2-D electron gas present at the AlGaN/GaN interface is employed as the bottom electrode as well as the transistor conducting channel. The carrier concentration of the channel is modulated when the device undergoes acoustic strain. A quality factor of 250 and acoustic transconductance of 25 μS is achieved at resonance frequency of 4.23 GHz, marking the highest frequency and highest transconductance reported to date for GaN-based RBTs. The frequency × Q of this device is among the best reported for GaN-based resonators.**

***Index Terms*— GaN, high electron mobility transistor (HEMT), microelectromechanical system (MEMS) resonator, Q, resonant body transistor (RBT).**

I. Introduction

GALLIUM NITRIDE (GaN) is proven to be the material of choice for high-frequency, high-power, and high-temperature applications owing to its wide bandgap and large breakdown electric field. GaN also offers a number of excellent mechanical properties such as strong piezoelectric and pyroelectric effects, high acoustic velocity, and superb mechanical and chemical stability, making it a suitable material for nano/microelectromechanical systems (NEMS/MEMS) [1]. High-performance GaN micromechanical resonators have been reported previously with frequencies mostly lower than 1.5 GHz [2], [3]. Extending the frequency of GaN resonators deeper into the gigahertz regime, where GaN ICs usually operate at, is hindered because of a large capacitive feedthrough between the input/output electrodes. Here, we introduce a thickness-mode resonant-body high electron mobility transistor (RB-HEMT), where we take advantage of the intrinsic HEMT current/voltage sensitivity to small changes in the channel charge. Polar heterostructure interfaces are shown to be very sensitive to built-in as well as external strain, where the change in the polarization because of strain is sensed through the current or voltage signal [4].

The concept of resonant body or resonant gate transistors (RBTs or RGTs) dates back to the introduction of the MEMS resonators [5]. In the past few years, research on RBTs was revived mostly using silicon (Si) as the resonating material [6]–[8]. One major difference between GaN RB-HEMTs and Si-based RBTs is the origin and the properties of the transistor conduction channel. Spontaneous and piezoelectric polarization create a fixed positive charge at the AlGaN/GaN interface. The positive sheet charge confines electrons at the AlGaN/GaN interface in a potential well, forming a 2-D electron gas (2-DEG) channel present at a zero gate voltage (normally ON). The origin of the conduction channel in the III-nitride HEMT structures suggests that they are very sensitive to mechanical stress, which changes the piezoelectric polarization-induced surface and interface charges. In Si-based transistors, however, the conduction channel is based on creating an inversion layer in the doped substrate by applying a gate voltage, which results in a higher scattering due to presence of parent atoms in the channel, higher $1/f$ noise, lower channel carrier mobility, and more pronounced electron scattering because of imperfections and surface roughness at the noncrystalline Si/SiO_2 interface. Above all, unlike Si-based FETs, GaN HEMTs make it possible to take advantage of piezoelectric actuation inherent in GaN material systems.

An AlGaN/GaN resonant HEMT was first demonstrated in [9] and was used to excite the flexural-mode resonance of a beam with frequencies in lower megahertz range. In this paper, we propose a single resonating HEMT that not only is the main vibrating element, but also is used to transduce the thickness-mode acoustic resonance (Fig. 1). We first proposed this structure in [3]; in this paper, we explain the design principle and report the measurement results of fabricated

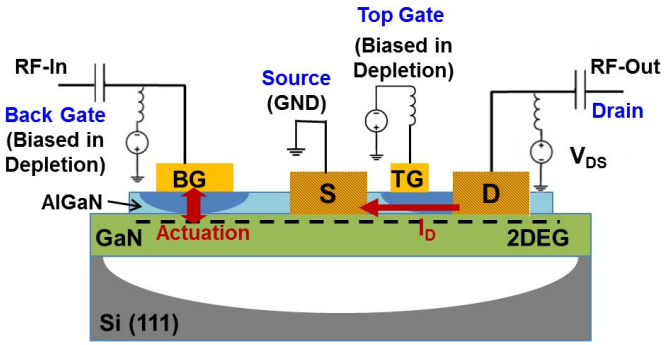

Fig. 1. Schematic view of AlGaN/GaN RB-HEMT. AC signal is applied to the back gate, which is biased in the depletion region (shown as the darker area under the back gate) for efficient transduction. 2-DEG, at the AlGaN/GaN interface, acts as the bottom electrode to piezoelectrically actuate the thickness resonance mode of the stack. The 2-DEG carrier density is modulated with the induced acoustic strain and reflected in the drain source current (I_D).

Manuscript received June 22, 2013; revised January 20, 2014; accepted January 21, 2014. This work was supported by the National Science Foundation under Award 1002036 and Award 1055308. The review of this paper was arranged by Editor G. Ghione.

The authors are with the Electrical Engineering and Computer Science Department, University of Michigan, Ann Arbor, MI 48109 USA (e-mail: azadans@umich.edu; minar@umich.edu).

Color versions of one or more of the figures in this paper are available online at http://ieeexplore.ieee.org.

Digital Object Identifier 10.1109/TED.2014.2302991

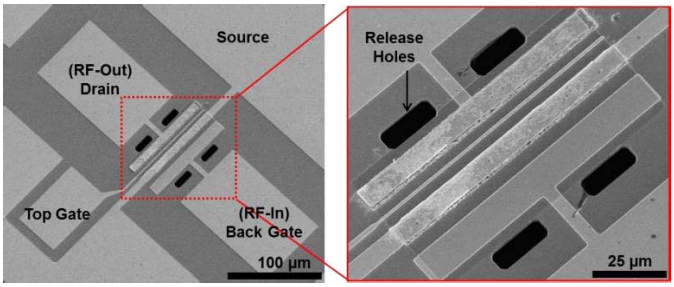

Fig. 2. SEM images of the AlGaN/GaN RB-HEMT with interdigitated fingers. Top gate length is 1 μm. The width of source and drain is 6 μm, and the back gate electrode is 8 μm wide.

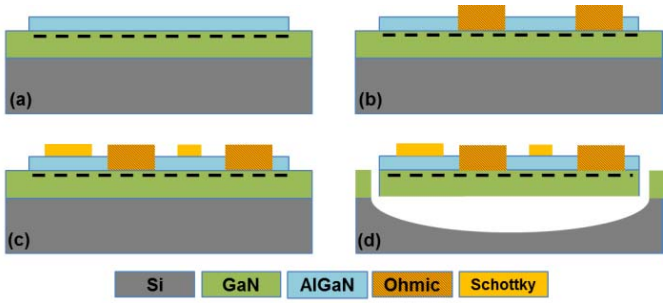

Fig. 3. Fabrication steps. (a) Mesa isolation. (b) Ohmic contact deposition and annealing. (c) Schottky contact formation. (d) Etching vias through GaN and XeF_2 isotropic etching of Si.

devices in detail. Unlike [9] and [10], where flexural resonance modes are excited by a HEMT actuator placed at one end of a suspended beam and read out through a separate HEMT at the other end, the proposed device is more compact, has higher electromechanical coupling using the thickness mode (e_{33}) piezoelectric coefficient, and operates at higher frequencies. Scanning electron microscope (SEM) images of a fabricated RB-HEMT are shown in Fig. 2.

RB-HEMTs can potentially be used in oscillators and frequency-shifting sensors to realize single-chip GaN-based integrated sensors and systems. The resonance frequency is set by the thickness of the stack and can be trimmed using mass loading or material removal as in the case of conventional film bulk acoustic resonators [12]. Their fabrication requires no modification to the HEMT baseline fabrication process with the exception of a single release step added as the final stage. These devices require no backside metallization and can be potentially solidly mounted on the substrate using proper acoustic wave reflectors placed underneath the main resonating body, eliminating the mechanical releasing step.

II. Fabrication

The RB-HEMTs are fabricated using metal-organic chemical vapor deposition (MOCVD) grown GaN-on-high-resistivity Si (111) as the starting wafer. Using GaN-on-Si wafers, one can take advantage of the mature Si technology. The total thickness of the GaN stack used in this paper is about 1.8 μm and the top AlGaN layer is 175-Å thick. More details on the stack can be found in [3].

The fabrication starts with defining the active area of the RB-HEMT by removing the 2-DEG outside of the mesa islands. Unlike [9] and [10], 2-DEG is only interrupted outside of the resonator active area; thus, better quality factors (Qs) can be achieved because of homogeneity in the mechanical structure. Ti/Al/Ti/Au is used for source and drain ohmic contact metallization followed by 30 s of annealing in nitrogen environment at 850 °C. Next, a Ni/Au layer is deposited to form the back gate Schottky contact (for acoustic actuation) and the top gate Schottky contact (for electrical modulation of the 2-DEG). Finally, vias were made through the GaN layer to access the Si layer, which is then isotropically etched by xenon difluoride (XeF_2). The fabrication process flow is shown in Fig. 3.

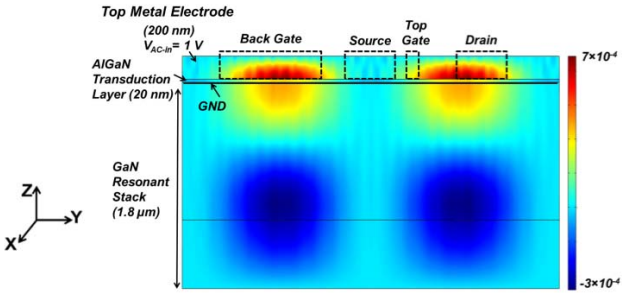

Fig. 4. COMSOL 2-D simulation of strain in the thickness direction (ε_z), showing the second-order thickness-mode resonance of GaN-based RB-HEMT. The AlGaN piezoelectric transduction layer is sandwiched between the back gate (top metal electrode) and the 2-DEG (bottom electrode). The simulation is used to define the electrode layout as shown in Fig. 2.

III. Principle of Operation

The thickness-mode resonance of the AlGaN/GaN RB-HEMT is effectively transduced using interdigitated electrodes. By optimizing the location of the fingers, different resonance modes or harmonics can be excited in the RB-HEMT. Given the stack mentioned earlier and using the electrode layout shown in Fig. 2, the fundamental thickness mode resonance at 2.12 GHz was excited showing a mechanical Q factor of 105 [13]. In this paper, we focus on the second-order thickness-mode resonance at 4.23 GHz with a Q factor of 250. The frequency $\times$ Q value of this device is 1.06×10^{12}, which is close to frequency $\times$ Q limit of GaN [1].

The proposed RB-HEMT is a four-terminal device consisting of a back gate Schottky contact to launch the acoustic wave into the device, a drain ohmic contact to sense the acoustic resonance, a source ohmic contact tied to zero potential to access the 2-DEG channel, placed at a nodal point, and an additional Schottky contact used for electrical modulation of the conducting channel (top gate). The simulated strain along the thickness of the device (z-direction) is obtained using COMSOL multiphysics simulation tool [14] in Fig. 4. An ac actuation voltage with amplitude of 1 V is applied to the top actuation electrode in the simulation defining the location of the back gate actuation contact. The source ohmic contact is utilized to access the 2-DEG channel (bottom electrode), and thus is placed in the middle of the structure with a minimum displacement. The modulated signal is the drain current, picked up from the drain contact. The maximum strain is induced at the top gate–drain region that changes the 2-DEG

sheet density and is in turn reflected as a change in the drain current.

The thin depleted AlGaN layer sandwiched between the back gate Schottky contact and the 2-DEG experiences a very high vertical electric field and is responsible for acoustic excitation of the entire 1.8-μm-thick AlGaN/GaN stack in the thickness direction, similar to piezoelectric actuation of standard metal–insulator–metal structures. The induced strain in the heterostructure is sensed through a change in the polarization at the AlGaN/GaN interface. The 2-DEG channel, under no external strain is originally formed because of a net polarization, composed of two components: 1) piezoelectric polarization in the strained AlGaN layer when grown pseudomorphically on GaN and 2) spontaneous polarization in AlGaN and GaN layers

$$+\sigma_B = \left(P_{\mathrm{SP}}^{\mathrm{AlGaN}} - P_{\mathrm{SP}}^{\mathrm{GaN}} + P_{\mathrm{PE}}^{\mathrm{AlGaN,Lattice}}\right) \cdot \hat{z} \qquad (1)$$

where $+\sigma_B$ is the interface sheet charge density, and $P_{\mathrm{SP}}^{\mathrm{AlGaN}}$ and $P_{\mathrm{SP}}^{\mathrm{GaN}}$ are the spontaneous polarization in the AlGaN and GaN layers, respectively, and $P_{\mathrm{PE}}^{\mathrm{AlGaN,Lattice}}$ is the piezoelectric polarization of the thin strained AlGaN layer. Note that there is no piezoelectric contribution from the 1.8-μm-thick GaN buffer layer, because the lattice of such thick stack is essentially relaxed and no strain is externally applied in this case. The effect of built-in AlGaN strain on the 2-DEG sheet density has been extensively investigated in [15], and in some cases AlGaN/GaN HEMTs have been reported as static strain sensors using the change in the 2-DEG sheet charge density [4] expressed by

$$\Delta\sigma_B = \left(P_{\mathrm{PE}}^{\mathrm{AlGaN,mech}} - P_{\mathrm{PE}}^{\mathrm{GaN,mech}}\right) \cdot \hat{z}. \qquad (2)$$

Using the same principle, in this paper, we take advantage of the change in interfacial sheet density at the AlGaN/GaN interface to sense bulk acoustic waves at higher frequencies. Using a FET-based sensing, the sensed signal no longer depends on the pickup electrode area and thus the device dimensions can be further scaled down to realize higher resonance frequencies with higher sensitivities.

IV. Measurement Results

The DC characteristics of the readout HEMT are measured using Keithly 4200-SCS parametric analyzer. RF measurements are carried out using an Agilent N5241A general-purpose network analyzer (PNA) with GSG ACP40 probes from Cascasde Microtech in a Lakeshore TTPX probe station. Short-open-load-through (SOLT) calibration was performed prior to all measurements. All measurements were taken with 50-Ω termination impedances.

A. DC Characteristics

As mentioned previously, the back gate Schottky contact is biased in the depletion region to avoid AlGaN layer degradation owing to current flow and to limit the conductivity of the AlGaN layer to the AlGaN/GaN interface. The DC characteristics of the back gate Schottky contact is shown in Fig. 5. The reverse Schottky region where the back gate is biased is shown in Fig. 5 inset.

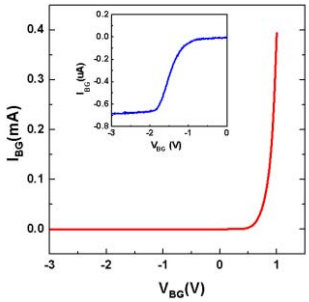

Fig. 5. Two-port I–V (conductance) measurement between the Schottky back gate and the source ohmic contact. A turn-on voltage of 0.75 V is measured for the Schottky contact. Inset: reverse Schottky region of operation, where the back gate is biased at. The back gate voltage approximately −1.9 V marks the value at which the 2-DEG is totally depleted (pinchoff voltage).

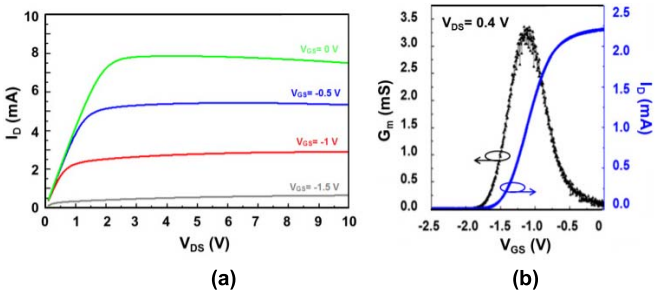

Fig. 6. DC response of the readout HEMT, consisting of the drain, top gate, and source (back gate is floating). The gate width is 100 μm. DC I–V transfer curves are plotted as (a) drain current (I_D) versus drain voltage at different gate voltage values (I_D–V_{DS}). The negative resistance at higher drain currents is associated with self-heating in the AlGaN/GaN HEMT channel. (b) Drain current and transconductance versus top gate voltage at $V_{\mathrm{DS}} = 0.4$ V.

The DC I–V transfer curves of the released HEMT are shown in Fig. 6. The three terminals of the RB-HEMT under measurement are the source, drain, and top gate. A threshold voltage of $\mathrm{V_{TH}} = -1.9$ V is observed for the readout HEMT.

Also noticeable in Fig. 6(b) is the strong dependence of readout HEMT transconductance (G_m) on the gate DC voltage, which is a characteristic of AlGaN/GaN HEMTs. One of the main reasons that results in reduction of transconductance at higher gate voltages is the nonlinear increase in the source-gate resistance with an increase in the drain current as the GaN velocity-field characteristic experiences early quasi-saturation [16]. The origin for the quasi-saturation in the electron velocity profile is generally associated with the high optical phonon energy in nitride-based semiconductors compared with that of other semiconductors, such as Si or GaAs. Different approaches have been considered to mitigate this problem by optimizing the design of GaN HEMTs [17], but is not the focus of our paper.

B. RF Measurements

The total transconductance of the RB-HEMT is extracted using (3), similar to the case of conventional transistors with the back gate set as Port 1 and the drain as Port 2

$$|Y_{21} - Y_{12}| = \sqrt{\left\{\mathrm{Real}\,(Y_{21} - Y_{12})\right\}^2 + \left\{\mathrm{Imag}\,(Y_{21} - Y_{12})\right\}^2}. \qquad (3)$$

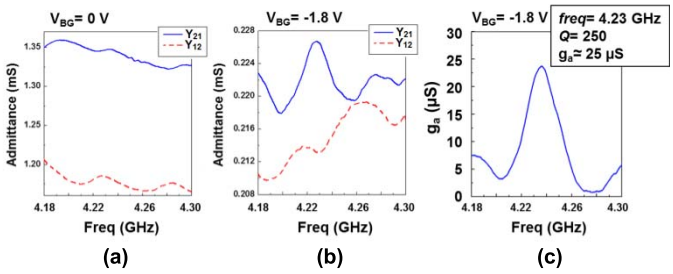

Fig. 7. Admittance parameters (Y_{21} and Y_{12}) are plotted at (a) $V_{\mathrm{BG}} = 0$ V and (b) $V_{\mathrm{BG}} = -1.8$ V. The resonance peak only appears in (b) where the 2-DEG under the back gate is depleted. (c) Acoustic transconductance (g_a) is extracted from (b). The second-order thickness-mode resonance at 4.23 GHz is excited, with a Q of 250 at $V_{\mathrm{BG}} = -1.8$ V. The electrical back gate feedthrough floor ($g_{\mathrm{mb}} = 0.043$ mS) is subtracted from $|Y_{21} - Y_{12}|$ to plot g_a. $V_{\mathrm{TG}} = -1$ V, and $V_{\mathrm{DS}} = 0.4$ V is kept constant in all the plots.

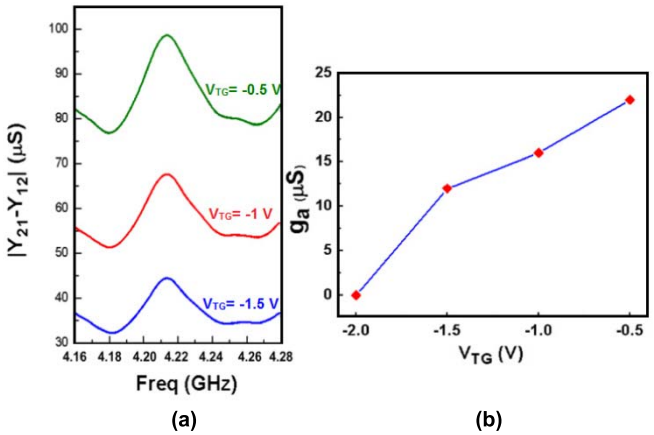

Fig. 8. (a) Total transconductance dependence on the top gate voltage ($V_{\mathrm{BG}} = -1.8$ V, $V_{\mathrm{DS}} = 0.4$ V). $|Y_{21} - Y_{12}|$ is plotted at different top gate voltages. The acoustic and back gate electrical transconductance decrease as the top gate DC voltage decreases. (b) Acoustic transconductance is plotted versus top gate DC voltage. The acoustic transconductance drops to zero when the channel is fully depleted (at $V_{\mathrm{TG}} = -2$ V).

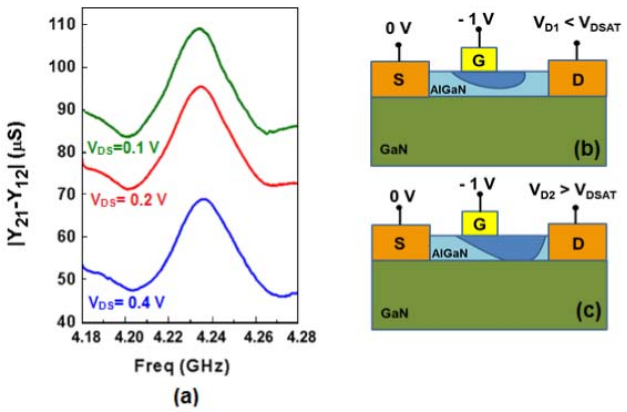

Fig. 9. (a) Total transconductance $|Y_{21} - Y_{12}|$ at different drain–source voltages in the linear region of operation. (b) Acoustic transconductance decreases as the depletion region grows toward the drain contact at higher V_{DS} values. (c) When the 2-DEG under the drain contacts gets pinched (SAT region), the acoustic transconductance value drops to zero. $V_{\mathrm{DS}} = 0.5$ V, corresponds to the knee voltage measured in Fig. 6(a), when $V_{\mathrm{TG}} = -1$ V, marking entering the saturation region of operation. The darker area in the AlGaN channel shows the depletion region, growing at higher V_{DS} values.

The total transconductance consists of a purely mechanical component (g_a) and an electrical broadband component (g_{mb}) related to the back gate electrical modulation. Fig. 7 shows Y_{21}, Y_{12}, and g_a plots with an input actuation power of $P_{\mathrm{in}} = -5$ dBm at two different back gate voltages: 1) $V_{\mathrm{BG}} = 0$ V and 2) $V_{\mathrm{BG}} = -1.8$ V. The back gate–source junction is further depleted in case 2) compared with case 1), resulting in lower Y_{21} and Y_{12} feedthrough levels. Furthermore, the acoustic resonance peak only appears in case 2), proving that the back gate Schottky contact acts as the top electrode and the 2-DEG as the bottom electrode, with the most effective actuation occurring when the AlGaN layer is depleted and the conduction path is limited to the AlGaN/GaN interface (i.e., at $V_{\mathrm{BG}} = -1.8$ V and $V_{\mathrm{ac}} = 0.1$ V resulting in: $V_{\mathrm{BG}} + V_{\mathrm{ac}} \approx V_{\mathrm{BG-pinchoff}}$) [9]. It is worth noting that large levels of feedthrough in the admittance plots are mainly due to the fact that the 2-DEG was kept uninterrupted within the resonating device and are mostly canceled out when the acoustic transconductance is extracted. The feedthrough level in both Y_{21} and Y_{12} plots can be significantly decreased by etching the 20-nm AlGaN layer from the unelectroded area between actuation and sense electrodes and thus removing the electric coupling between the back gate and the drain contact.

In Fig. 7(c), g_a is extracted by subtraction of the back gate electrical transconductance ($g_{\mathrm{mb}} = 0.043$ mS) from the total transconductance value ($|Y_{21} - Y_{12}|$). g_a rises to $\sim$25 μS with a very small off-resonance signal level.

It must be noted that the RB-HEMT acoustic transconductance is measured from the back gate to the drain and does not follow the trend of the readout HEMT transconductance curve, measured from the top gate to the drain [shown in Fig. 6(b)]. This can be explained by the transduction mechanism and the physics of the device. The 2-DEG carrier density is locally modulated only in the drain access region, where maximum strain is induced (shown in Fig. 4). Thus, the change in the sheet density is not uniform along the entire HEMT channel. The acoustic transconductance is calculated and its relation with the transistor transconductance is derived in Section VI.

The depletion region between the top gate and the drain grows wider as the voltage difference between them increases, thus narrowing the conducting channel and lowering admittance values between the back gate and the drain. Hence, at a fixed drain voltage, as the top gate voltage becomes more negative, g_a and g_{mb} both drop. Fig. 8 shows the RB-HEMT transconductance versus the top gate voltage at $V_{\mathrm{DS}} = 0.4$ V.

Similarly, at a fixed top gate voltage, as the drain voltage increases, the depletion region width increases at the drain side, resulting in lower 2-DEG carrier concentration, until the channel gets pinched [Fig. 9(a)]. As mentioned before, the detection mechanism relies on modulation of the 2-DEG carrier concentration in the top gate–drain region. Therefore, the most effective modulation occurs when the channel under the top gate–drain is conducting. At $V_{\mathrm{DS}} = V_{\mathrm{DS(sat)}}$, the 2-DEG on the drain side gets pinched and its carrier concentration can no longer be modulated by the induced acoustic strain on the drain side; therefore, $|Y_{21} - Y_{12}|$ drops significantly [Fig. 9(c)].

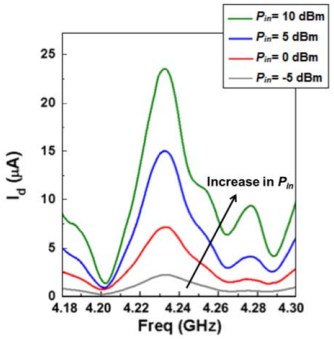

Fig. 10. Frequency response of the drain motional current ($g_a \times V_{bg}$) of the RB-HEMT. As the input RF power increases, the motional current increases. Nonlinear effects start to show up at higher P_{in} values.

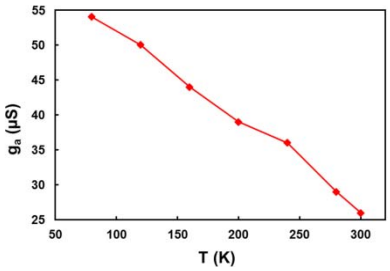

Fig. 11. Temperature trends of the acoustic transconductance of a RB-HEMT at $V_{BG} = -1.8$ V, $V_{TG} = 0$ V, and $V_{DS} = 0.2$ V. The acoustic transconductance decreases from $g_a = 53$ μS at 80 K to $g_a = 25$ μS at 300 K.

Fig. 10 shows the dependence of the drain motional current on the input RF power applied to the back gate. As the input ac actuation voltage increases, the strain induced in the heterostructure increases, resulting in larger polarization and sheet density induced at the AlGaN/GaN interface, and therefore an increase in the motional current. However, the back gate–source depletion width and thus actuator depletion capacitance gets modulated with applied input ac voltage. Particularly, nonlinearity is introduced in the response at larger input ac voltages. At $P_{in} = 10$ dBm, the acoustic current starts to saturate as shown in Fig. 10. Furthermore, the reflection of the incident power from Port 1 of the PNA determines the effective actuation voltage at the input of the RB-HEMT. Hence, matching conditions vary at different RF input power levels, which is another source of nonlinearity in the motional current.

C. Effect of Temperature

Fig. 11 shows the effect of temperature on the acoustic transconductance of an RB-HEMT. We previously studied the effect of temperature on the DC characteristics of our fabricated GaN HEMTs [3], where a decrease in the HEMT drain current and transconductance values were observed with an increase in temperature. 2-DEG mobility has a strong temperature dependence, and it decreases at higher temperatures because of an increase in various scattering mechanisms [18]. Therefore, degradation in the transduction efficiency of GaN RB-HEMTs is expected with an increase in temperature, as shown in Fig. 11. GaN RB-HEMTs, similar to other GaN BAW resonators, exhibit a negative temperature coefficient of frequency [1], [2].

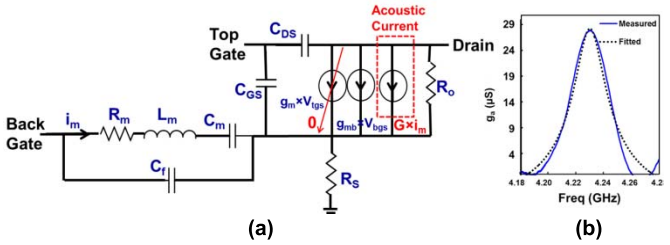

Fig. 12. (a) Equivalent electrical circuit model of the four-terminal RB-HEMT. AC signal is fed to the back gate and collected from the drain. The actuation takes place between the back gate and the source. The induced acoustic wave modulates the drain current. At the resonant frequency, $i_m = V_{in}/R_m$, and $g_a = i_{out}/V_{in}$, therefore G can be written as: $G = g_a \times R_m$. (b) Measured and fitted g_a at $V_{TG} = 0$ V and $V_D = 0.2$ V.

TABLE I
EXTRACTED VALUES OF THE EQUIVALENT CIRCUIT COMPONENTS AT $V_{TG} = 0$ V AND $V_D = 0.2$ V

Parameter	$R_m(\Omega)$	$L_m(\mu H)$	$C_m(fF)$	$C_f(pF)$
Extracted Value	147	1.38	1.025	1.59
Parameter	G	$C_{GS}(pF)$	$C_{GD}(pF)$	$R_o(\Omega)$
Extracted Value	0.005	0.42	0.3	500

V. SMALL SIGNAL MODEL

Equivalent circuit model of the RB-HEMT is shown in Fig. 12(a). The acoustic actuator is modeled with its Butterworth Van Dyke equivalent circuit. The motional branch (R_m, L_m, and C_m) is located between the back gate and source since the actuation is through the back gate Schottky top electrode and the source ground electrode [19]. The parallel capacitance (C_f) models the parasitic static capacitance of the actuator.

To model the acoustic current, a current-controlled current-source is used with reference to [20], which senses the input motional current, i_m, and multiplies it by a unit-less factor of G. At the resonance frequency, G is equal to $R_m \times g_a$. R_m is the motional resistance and g_a is the acoustic transconductance. g_{mb} represents the broadband electrical transconductance from the back gate to the drain. The acoustic, g_a, back gate electrical, g_{mb}, and top gate electrical, g_m, transconductances are all dependent on the top gate DC voltage, as discussed earlier. Fig. 12(b) compares the measured response with the fitted one using the proposed electrical model. The fitted component values are listed in Table I.

VI. DISCUSSION

In this section, the acoustic transconductance is analytically derived and compared with the measurement results. As discussed previously, under external strain, piezoelectric

polarization fields in the AlGaN and GaN layer change; therefore, a change in the 2-DEG sheet density is expected. Piezoelectric polarization induced along the thickness of a piezoelectric material when a voltage of V_z is applied across its thickness is [21]

$$P_Z = V_Z \times \varepsilon_0 \varepsilon_r / d. \tag{4}$$

With $\Delta V_Z = 0.1$ V applied across the AlGaN actuation layer, AlGaN dielectric constant (ε_r) of 9, and AlGaN thickness (d) of 200 Å, polarization along the thickness of the AlGaN actuation layer is calculated as

$$P_Z^{\text{AlGaN}} = 3.98 \times 10^{-4}\ \text{C/m}^2. \tag{5}$$

The induced strain in the thickness direction can be calculated from the polarization field by

$$\varepsilon_Z = P_Z / e_{33} \tag{6}$$

where e_{33} is the thickness-mode piezoelectric constant, which is estimated for $Al_xGa_{(1-x)}N$ alloy according to Vegard's law [15] as

$$e_{ij}^{\text{AlGaN}} = x.e_{ij}^{\text{AlN}} + (1-x)e_{ij}^{\text{GaN}}. \tag{7}$$

Using piezoelectric constants of GaN and AlN from [15] ($e_{33}^{\text{GaN}} = 0.7$ C/m^2, and $e_{33}^{\text{AlN}} = 1.4$ C/m^2) and an Al mole fraction (x) of 0.3, e_{33}^{AlGaN} is found to be 1.03 C/m^2.

Therefore, the strain in z-direction (ε_Z) in the actuator area is calculated to be 3.86×10^{-4} using P_Z and e_{33} of AlGaN calculated above with $V_z = 0.1$ V, which is about 10× smaller than the simulated strain for $V_z = 1$ V shown in Fig. 4.

The effective induced strain on the sense area (ε'_z), which is smaller than ε_z, creates a polarization in the AlGaN/GaN interface owing to their different piezoelectric constants as

$$P_z = \varepsilon'_z.\left(e_{33}^{\text{AlGaN}} - e_{33}^{\text{GaN}}\right) + 2\varepsilon'_y.\left(e_{31}^{\text{AlGaN}} - e_{31}^{\text{GaN}}\right). \tag{8}$$

Yielding a change is piezoelectric polarization of $P_{z,\text{interface}} = 1.3 \times 10^{-4}$ C/m^2, or equivalently a sheet density change $[d(n_s)]$ of 8×10^{14}/m^2. Please note that the first term in (8) is dominant and the in-plane strain is neglected.

As shown in the COMSOL simulation in Fig. 4, the strain is induced effectively only at top-gate-drain region, and does not affect the entire channel of the readout HEMT. Thus, the contribution of each region with a different strain profile in the readout HEMT is considered separately. To find the change in the drain current, we define three regions in the readout HEMT as the source, drain access regions, and the intrinsic HEMT channel (Fig. 13).

The change in the drain current owing to change in the channel resistance is

$$d(I_D) = d\left(\frac{V_{\text{DS}}}{R_{\text{ch,ext}}}\right) = -d(R_{\text{ch,ext}}) \times \frac{V_{\text{DS}}}{(R_{\text{ch,ext}})^2} \tag{9}$$

where $R_{\text{ch,ext}}$ is the extrinsic channel resistance comprising of

$$R_{\text{ch,ext}} = R_S + R_D + R_{\text{ch}} \tag{10}$$

where R_S and R_D are the source and drain access resistances and R_{ch} is the intrinsic HEMT channel resistance expressed by

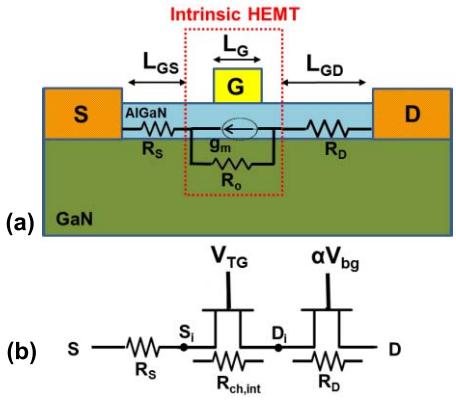

Fig. 13. (a) Structure of the readout HEMT, showing the source and drain access regions and the intrinsic HEMT. (b) External strain in the channel is induced from the back gate actuator, and effectively modulates the sheet density of the drain access region only. The drain access resistance can be equivalently modeled as a transistor [22], where the channel resistance is modulated with the back gate voltage. The voltage drop at the drain and source access regions, results in effective voltages of V_{Di} and V_{Si} at the intrinsic HEMT drain and source terminals.

$$R_{\text{ch}} = \frac{L_G}{Wq\mu n_{S,\text{ch}}} \tag{11}$$

$$R_S = R_c + \frac{L_{\text{GS}}}{Wq\mu n_S} \tag{12}$$

$$R_D = R_c + \frac{L_{\text{GD}}}{Wq\mu n_S}. \tag{13}$$

L_G, L_{GS}, and L_{GD} are the gate length, gate–source, and gate–drain spacing, respectively, shown schematically in Fig. 13. As the strain is only induced in the drain–gate region with this design, the change in the external resistance becomes

$$d(R_{\text{ch,ext}}) = d(R_D) = -d(n_S) \times \frac{L_{\text{GD}}}{Wq\mu n_S^2}. \tag{14}$$

Thus, (9) can be rewritten as

$$d(I_D) = d(n_S) \frac{\frac{L'_{\text{GD}}}{Wq\mu n_S^2}}{\left(\frac{L_{\text{GS}}+L_{\text{GD}}}{Wq\mu n_S} + \frac{L_G}{Wq\mu n_{S,\text{ch}}}\right)^2} \times V_{\text{DS}} \tag{15}$$

where $n_{S,\text{ch}}$ is the sheet density in the intrinsic HEMT channel, which is dependent on the HEMT biasing and n_S is the sheet density at the drain and source access regions. The mobility used in the above equation is the average electron mobility in the channel at low electric fields.

Note that L_{GD} in (14), has been replaced with L'_{GD} in (15), to account for the depletion width modulation with increased drain voltage. As the drain voltage increases, the depletion region between the gate and drain grows wider and the effective L_{GD} decreases. Thus, the sense area or the drain access region in the readout HEMT decreases, which reduces the $d(I_D)$. Therefore L'_{GD} is defined as the effective gate–drain access region length, by considering the effect of depletion width modulation at higher drain voltages.

In the linear region of operation, at open channel condition, we assume the sheet density is constant for the three regions of

TABLE II
COMPARISON BETWEEN RESONANCE FREQUENCY, Q, AND TRANSCONDUCTANCE (g_a) OF Si AND GaN-BASED RESONANT TRANSISTORS

Ref.	*Material*	*Frequency*	*Q*	g_a
[6]	Si	14.3 MHz	700	-
[7]	Si	71.3 MHz	13200	-
[8]	Si	11.7 GHz	1830	15 μS
[9]	AlGaN/GaN	1.3 MHz	226	6 μS
[11]	AlGaN/GaN	2.67 GHz	650	6 μS
[13]	AlGaN/GaN	2.1 GHz	105	15.5 μS
This Work	AlGaN/GaN	4.23 GHz	250	> 25 μS

HEMT to calculate the acoustic transconductance. Therefore, the acoustic transconductance, g_a, defined as

$$g_a = \frac{d(I_D)}{d(V_{\mathrm{BG}})} \tag{16}$$

and is calculated to be 32 μs using $L_{\mathrm{GD}} = 4\ \mu$m, $L_G = 1\ \mu$m, $L_{\mathrm{GS}} = 3\ \mu$m, average electron mobility $\mu_n = 300$ cm^2/v.s, $V_{\mathrm{DS}} = 0.1$ V, and $V_{\mathrm{BG}} = 0.1$ V. The calculated value of g_a is slightly larger than measurement data for acoustic transconductance ($g_a = 27\ \mu$S) shown in Fig. 10 (g_a). The small discrepancy is attributed to the growth-dependent values of piezoelectric coefficients of GaN and AlGaN, material loss, smaller effective induced strain in the channel at the sense area than actuation, and the fact that the depletion width modulation is not considered in our calculations (i.e., $L'_{\mathrm{GD}} < 4\ \mu$m). From this analysis, it is clear that to get maximum acoustic transconductance, one has to place the drain and source contact across the region of maximum strain.

VII. CONCLUSION

A multigigahertz RB-HEMT was demonstrated in this letter, which exhibits the second-order thickness-mode resonance frequency of 4.23 GHz with a Q factor of 250. Cointegrated with GaN ICs, the proposed RB-HEMT can potentially offer all-GaN integrated nano/microsensors and systems. The resonance frequency can be further increased by exciting higher harmonics of the thickness mode; however, in this paper, because of the large back gate periphery and thus high capacitive and electrical feedthrough overwhelming the acoustic transconductance, the frequency was limited to less than 6 GHz. Higher resonant frequencies can be excited by scaling the device dimensions further into the nanometer scale. Furthermore, using an optimized design, the RB-HEMT can operate in the saturation region and take advantage of the intrinsic amplification of the HEMT. The proposed RB-HEMT is the first step toward the realization of a resonant transistor that can offer similar advantages as its Si counterparts but in a piezoelectric GaN-based material system (see Table II).

ACKNOWLEDGMENT

The authors would like to thank staff at the University of Michigan Lurie Nanofabrication Facility, a member of NNIN and Prof. J. Singh of University of Michigan for helpful discussion.

REFERENCES

[1] V. J. Gokhale, J. Roberts, and M. Rais-Zadeh, "High-performance bulk-mode gallium nitride resonators and filters," in *Proc. 16th Int. Solid-State Sensors, Actuat. Microsyst. Conf.*, Beijing, China, 2011, pp. 926–929.
[2] A. Ansari, V. J. Gokhale, V. A. Thakar, J. Roberts, and M. Rais-Zadeh, "Gallium nitride-on-silicon micromechanical overtone resonators and filters," in *Proc. IEEE IEDM*, Washington, DC, USA, Dec. 2011, pp. 485–488.
[3] A. Ansari, V. Gokhale, J. Roberts, and M. Rais-Zadeh, "Monolithic integration of GaN-based micromechanical resonators and HEMTs for timing application," in *Proc. IEEE IEDM*, San Francisco, CA, USA, Dec. 2012, pp. 15.5.1–15.5.4.
[4] Y. R. Wu and J. Singh, "Polar heterostructure for multifunction devices: Theoretical studies," *IEEE Trans. Electron Devices*, vol. 52, no. 2, pp. 284–293, Feb. 2005.
[5] H. C. Nathanson, W. E. Newell, R. A. Wickstrom, and J. R. Davis, "The resonant gate transistor," *IEEE Trans. Electron Devices*, vol. 14, no. 3, pp. 117–133, Mar. 1967.
[6] C. Durand, F. Casset, P. Renaux, N. Abele, B. Legrand, D. Renaud, *et al.*, "In-plane silicon-on-nothing nanometer-scale resonant suspended gate MOSFET for in-IC integration perspectives," in *Proc. IEEE Electron Device Lett.*, vol. 29, no. 5, pp. 494–496, May 2008.
[7] D. Grogg, M. Mazza, D. Tsamados, and A. M. Ionescu, "Multi-gate vibrating-body field effect transistor (VB-FETs)," in *Proc. IEEE IEDM*, San Francisco, CA, USA, Dec. 2008, pp. 1–4.
[8] D. Weinstein and S. A. Bhave, "The resonant body transistor," *Nano Lett.*, vol. 10, no. 4, pp. 1234–1237, Feb. 2010.
[9] M. Faucher, B. Grimbert, Y. Cordier, N. Baron, A. Wilk, H. Lahreche, *et al.*, "Amplified piezoelectric transduction of nanoscale motion in gallium nitride electromechanical resonators," *Appl. Phys. Lett.*, vol. 94, no. 23, p. 233506, Jun. 2009.
[10] M. Faucher, Y. Cordier, M. Werquin, L. Buchaillot, C. Gaquiere, and D. Theron, "Electromechanical transconductance properties of a GaN MEMS resonator with fully integrated HEMT transducers," *J. Micromech. Syst.*, vol. 21, no. 2, pp. 370–378, Apr. 2012.
[11] L. Popa and D. Weinstein, "Switchable piezoelectric transduction AlGaN/GaN MEMS resonators," in *Proc. 17th Int. Conf. Solid-State Sensors, Actuat. Microsyst.*, Barcelona, Spain, Jun. 2013, pp. 2461–2464.
[12] H. Campanella, "Tunable FBARs: Frequency tuning mechanisms," in *Proc. 40th Eur. Microw. Conf.*, Paris, Sep. 2010, pp. 795–798.
[13] A. Ansari and M. Rais-Zadeh, "HEMT-based read-out of a thickness-mode AlGaN/GaN Resonator," in *Proc. IEEE IEDM*, Washington, DC, USA, Nov. 2013, pp. 1–4.
[14] (2013, Jun. 20). *COMSOL Home Page* [Online]. Available: http://www.comsol.com/
[15] O. Ambacher, B. Foutz, J. Smart, J. R. Shealy, N. G. Weimann, K. Chu, *et al.*, "Two dimensional electron gases induced by spontaneous and piezoelectric polarization in undoped and doped AlGaN/GaN heterostructures," *J. Appl. Phys.*, vol. 87, no. 1, pp. 334–344, Jan. 2000.
[16] Y. R. Wu, M. Singh, and J. Singh, "Sources of transconductance collapse in III–V nitrides-consequences of velocity-field relations and source/gate design," *IEEE Trans. Electron Devices*, vol. 52, no. 6, pp. 1048–1054, Jun. 2005.
[17] T. Palacios, S. Rajan, A. Chakraborty, S. Heikman, S. Keller, S. P. DenBaars, *et al.*, "Influence of the dynamic access resistance in the g_m and f_T linearity of AlGaN/GaN HEMTs," *IEEE Trans. Electron Devices*, vol. 52, no. 10, pp. 2117–2123, Oct. 2005.
[18] D. Jena, "Polarization induced electron populations in III-V nitride semiconductors transport, growth, and device applications," Ph.D. Thesis, Dept. Electr. Eng., Univ. California, Santa Barbara, CA, USA, 2003.
[19] E. Hwang, A. Driscoll, and S. Bhave, "A platform for JFET-based sensing for RF MEMS resonators in CMOS technology," in *Proc. IEEE IEDM*, Washington, DC, USA, Dec. 2011, pp. 489–492.
[20] C. Nguyen and R. T. Howe, "An integrated CMOS micromechanical resonator high-Q oscillator," *IEEE J. Solid-State Circuits*, vol. 34, no. 4, pp. 440–455, Apr. 1999.
[21] A. Arnau Vives, *Piezoelectric Transducers and Applications*. 2nd ed. New York, NY, USA: Springer-Verlag, 2008.
[22] U. Radhakrishna, "A compact transport and charge model for GaN-based high electron mobility transistors for RF applications," M.S. thesis, Dept. Electr. Eng. Comput. Sci., Massachusetts Inst. Technol., Cambridge, MA, USA, Jun. 2013.

Azadeh Ansari (S'10) received her B.S. degree in Electrical Engineering from Sharif University of Technology, Tehran in 2010. Currently, she is pursuing her Ph.D. degree at the University of Michigan, Ann Arbor.

Her research interests include GaN-based micromechanical resonators, resonant transistors, oscillators, and interface circuit design for MEMS.

Mina Rais-Zadeh (S'03–M'08–SM'12) received her Ph.D. in Electrical and Computer Engineering from Georgia Institute of Technology in 2008. Since January 2009, she has been with the University of Michigan, Ann Arbor, where she is currently an Assistant Professor in the Electrical Engineering Department.

Her research interests include RF MEMS, passive micromachined devices for communication applications, gallium nitride MEMS, resonant sensors, and micro/nano fabrication process development.